International Journal of Fluid Power 1 (2000) No. 1 pp. 17-25

# STATIONARY AXIAL FLOW FORCE ANALYSIS ON COMPENSATED SPOOL VALVES

**M. Borghi[1], M. Milani[1], R. Paoluzzi[2]**

[1] *Engineering Science Department - University of Modena - Via Campi 213/b - 41100 Modena – Italy*
[2] *CEMOTER – Italian National Reseach Council - Via Canal Bianco, 28 - 44044 Cassana - Ferrara – Italy*
*borghi.massimo@unimit, milani@omero.dsi.unimo.it, paoluzzi@cemoter.bo.cnr.it*

**Abstract**

The paper deals with an application of a simplified numerical analysis, based on Computational Fluid Dynamics (CFD), of the flow field inside the compensated port connections of a reference spool valve. The aim of the study was to evaluate a proposed analysis procedure, for the major effects related to the presence of steady state flow forces affecting the spool equilibrium. Starting from an initial summary of the dimensional analysis proposed by the authors to approach the application of CFD to hydraulic components, the paper presents the results of three commonly used compensating profiles for two reference spool positions. In order to validate the simulation, the curves obtained for one of the three geometries are compared with the experimental data obtained on an equivalent port connection of a commercial distributor.

**Keywords:** CFD simulation, compensated spool valves, steady state flow forces

## 1 Introduction

The solution of the turbulent field described by various equations derived from the classic Navier-Stokes equation, is one of the most challenging problems in numerical simulation. The techniques available, generally require tremendous investments in terms of hardware, software and time, in order to be applied with success to real world engineering problems. Fluid power components in general, and hydraulic valves in particular, on this aspect are penalized by the relatively small monetary value of the component, which make the existence of a breakeven point in the cost/benefit analysis questionable.

On the other hand, hydraulic valves have some benefits, which can be used in order to try to improve the effectiveness of a CFD run. Geometries are often axis-symmetric in the region where the pressure drop occurs; the turbulence characteristics are such that the discharge of the fluid through the metering edge can be approximated by quadratic laws; and, last but not least, dimensional analysis improves the general validity of flow simulations.

When these aspects are considered in the light of the increasing computational power available in an ever growing computer environment, the perspective opened to the engineering application of CFD on valve design is definitely brighter than just a few years ago.

The application of the analysis procedure to investigate the axial flow forces in compensated profiles is a further step in the direction of the introduction of CFD in the main stream of design procedures in the technical department of fluid power components manufacturers.

This manuscript was received on 25 November 1999 and was accepted after revision for publication on 31 January 2000

## 2 Theoretical Approach

Among the forces acting on the mobile element of hydraulic valves, and contributing to its equilibrium, a fundamental role is played by flow forces. They are an effect of the momentum change in fluid under the action of a pressure gradient. If the valve geometry is so designed to compensate, at least partially as in Fig. 1, for their effect, the fluid flows from regions with high pressure to regions with low pressure with a first change in momentum at the metering edge. A second change occurs where the spool is machined to induce a momentum variation aimed at compensating the flow force effect.

Provided that:

- the hypothesis of inviscid and incompressible fluid holds;
- the efflux geometry can be considered two dimensional;

- the flux is irrotational in regions close to the metering edge;

it is possible to estimate the axial flow force in a compensated spool (Blackburn et al 1960 and Merrit 1967) as:

$$F = \rho \cdot \frac{Q^2}{C_c \cdot A_{TH}} \cdot (\cos\theta_1 - \cos\theta_2) \qquad (1)$$

where $Q$ is the flow rate crossing the port, $C_C$ *vena contracta* coefficient, $A_{TH}$ is the theoretical cross sectional area, $\theta_1$ and $\theta_2$ are the flow jet angles at the metering and compensating section respectively.

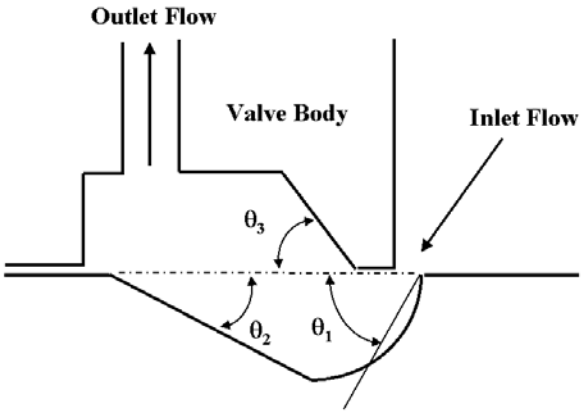


**Fig. 1:** *Efflux angles in a compensating connection.*

Using the commonly accepted definitions for the discharge coefficient $C_d$ and the velocity coefficient $C_v$, the following equations hold:

$$C_d = C_v \cdot C_c \qquad (2)$$

$$C_v = \frac{U_{TH}}{U_R} \qquad (3)$$

where $U_R$ indicates the maximum fluid velocity at the discharge section. If the efflux can be considered fully turbulent with a completely developed velocity profile (i.e. $Re$ > 100÷400), reminding that:

$$Q = C_d \cdot A_{TH} \cdot \sqrt{\frac{2 \cdot \Delta p}{\rho}} \qquad (4)$$

the *vena contracta* coefficient can be written in the form:

$$C_c = \frac{C_d}{C_v} = \frac{Q}{A_{TH} \cdot U_{TH}} \cdot \frac{U_R}{\sqrt{\frac{2 \cdot \Delta p}{\rho}}} \qquad (5)$$

The theoretical mean velocity of the fluid at the metering section can be written as a function of the flow rate crossing the compensated metering section $Q$ and its cross sectional area $A_{TH}$ :

$$U_{TH} = \frac{Q}{A_{TH}} \qquad (6)$$

Considering the equations above, Eq. (1) can be rewritten in the form:

$$F = \rho \cdot \frac{Q^2}{U_R \cdot A_{TH}} \cdot \sqrt{\frac{2 \cdot \Delta p}{\rho}} \cdot (\cos\theta_1 - \cos\theta_2) \qquad (7)$$

In Equation (7), the axial flow force value is made dependent on known and measurable quantities (flow rate, pressure drop, fluid density, cross sectional area and compensating profile angle) on one hand, and quantities known only once the flow field is solved (actual out-stream velocity or jet stream angle) on the other.

Quantities belonging to this last category can be computed only with an extensive use of Computational Fluid Dynamics tools, able to solve the complex Navier-Stokes equations and to visualize the flow field.

Past articles (Borghi et al 1997) showed how the flow characteristics of complex geometry can be dramatically simplified using axis-symmetric approaches and making an extensive use of non-dimensional techniques for problems formulation. On one hand this allows a reduction of the time needed to solve the equations, and on the other to preserve the fundamental information on the flow field and the derived variables (as for instance the axial flow force).

As it is well known, the non-dimensional statement of a fluid flow problem requires the definition of a length, a speed (or as an alternative a time) scale and therefore a Reynolds number defining the problem. These reference values define the scale factors for all the derived quantities, and therefore:

$$F^* = \frac{F}{C_F}; \quad Q^* = \frac{Q}{C_Q}; \quad \Delta p^* = \frac{\Delta p}{C_P}$$

$$U^* = \frac{U}{C_U}; \quad A^* = \frac{A}{C_A} \qquad (8)$$

Equation (7) can be rewritten introducing dimensionless variables defined by the scale factors above:

$$F^* \cdot C_F = \rho \cdot \frac{(Q^* \cdot C_Q)^2}{U_R^* \cdot C_U \cdot A_{TH}^* \cdot C_A} \cdot \sqrt{\frac{2 \cdot \Delta p^* \cdot C_p}{\rho}} \cdot (\cos\theta_1 - \cos\theta_2) \qquad (9)$$

$$F^* = \frac{Q^{*2}}{U_R^* \cdot A_{TH}^*} \cdot \sqrt{\Delta p^*} \cdot (\cos\theta_1 - \cos\theta_2) \cdot \left( \frac{\rho \cdot C_Q^2}{C_F \cdot C_U \cdot C_A} \cdot \sqrt{\frac{2 \cdot C_p}{\rho}} \right) \qquad (10)$$

Following the approach fully referenced in (Borghi, Cantore et al 1998), the scale factors are defined as a function of reference values (indicated by the subscript $_{REF}$), as summarized below:

$$C_A = L_{REF}^2 \qquad (11)$$

$$C_U = v \cdot Re_{REF} \cdot L_{REF}^{-1} \qquad (12)$$

$$C_Q = C_A \cdot C_Q = v \cdot Re_{REF} \cdot L_{REF} \qquad (13)$$

$$C_P = \rho \cdot v^2 \cdot Re_{REF}^2 \cdot L_{REF}^{-2} \qquad (14)$$

$$C_F = \rho \cdot v^2 \cdot Re_{REF}^2 \qquad (15)$$

This introduces a simplification for the term in

brackets of Eq. (9):

$$\left(\frac{\rho \cdot C_Q^2}{C_F \cdot C_U \cdot C_A} \cdot \sqrt{\frac{2 \cdot C_p}{\rho}}\right) = \rho \cdot \frac{v^2 \cdot Re_{REF}^2 \cdot L_{REF}^2}{\rho \cdot v^2 \cdot Re_{REF}^2 \cdot \nu \cdot Re_{REF} \cdot L_{REF}^{-1} \cdot L_{REF}^2} \cdot \sqrt{\frac{2}{\rho} \cdot \rho \cdot v^2 \cdot Re_{REF}^2 \cdot L_{REF}^2} = \sqrt{2} \quad (16)$$

and therefore the non-dimensional form of Eq. (1) becomes:

$$F^* = \sqrt{2} \cdot \frac{Q^{*2}}{U_R^* \cdot A_{TH}^*} \cdot \sqrt{\Delta p^*} \cdot (\cos\theta_1 - \cos\theta_2) \quad (17)$$

Equation (17) is directly derived from Eq. (7), with the only remarkable difference that the non-dimensional variable used in the simplified CFD model are in evidence. The solution of this model gives the non-dimensional values of flow rate, pressure drop, velocity module and angle ready to be used for non-dimensional force computation. Moreover, with reference to the approach presented by Borghi, Cantore et al (1998), the non-dimensional result obtained for a given spool position and a given Reynolds number, can be extended to a full range of operating characteristics at fixed spool position, provided that the turbulence approximation implied by Eq. (4) is valid. With a single numerical run, a determination of a general *F-Δp* characteristic at given spool position can be possible.

This can be done considering the dimensional stationary axial flow force computed for a given Reynolds number of the flow $Re_{REF}$ as:

$$F = C_F \cdot F^* \quad (18)$$

the axial flow force in a different flow rate condition is therefore given by:

$$F_1 = \beta^2(Re) \cdot F \quad (19)$$

where a conversion factor related to the flow Reynolds number is defined as:

$$\beta(Re) = \frac{Re_1}{Re_{REF}} \quad (20)$$

In the reminder of the paper, the approach outlined will be applied to three different compensated geometry in order to evaluate their ability to minimize the total axial flow force. The numerical results are also compared to experimental evidence in order to validate the models and confirm tendencies already shown for non-compensated geometry (Borghi et al 1997).

## 3 Numerical Models

The CFD analysis of the flow field was performed on three different compensated spool profiles.

The three dimensional geometry was approximated by an axis-symmetric model having radial inlet and outlet. The reference situation shown in Fig. 2 has a chamber rounding the edge close to the metering section with a radius equal to the spool chamber radial opening, and a straight compensating profile at the outlet inclined at 45°.

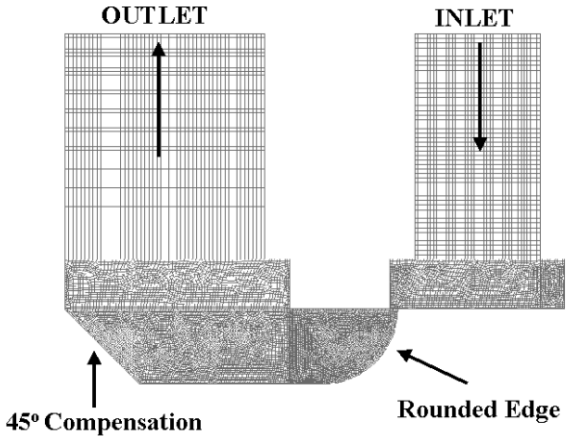


**Fig. 2:** *CFD Mesh used to represent the actual geometry of the compensated connection experimentally characterised (Case **A**)*

This model (case A) was chosen as a reference geometry for this study due to its similarity with the actual characteristic of a commercial distributor. The distributor was object of an extensive test investigation, and its *F-Δp* characteristic was hereby known for a number of different openings.

In order to improve the generality of the results shown, two different compensating geometries, derived from the one shown in Fig. 2, have been investigated, and are shown in Fig. 3.

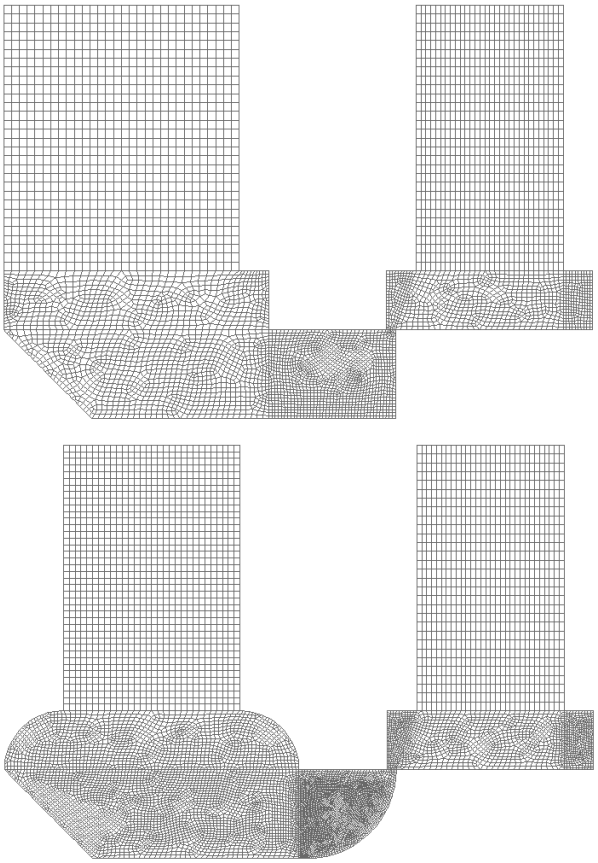

**Fig. 3:** *Modified geometry considered for CFD analysis. Case **B**, left, and Case **C**, right.*

The first derived geometry has a sharp 90° edge with no chamfer (case B), and the second has a circulating chamber engraved in the valve land at the outlet section (case C).

All the geometries have been meshed using quadrilateral four-nodes elements, mixing structured and unstructured grids in order to have a final mesh able to follow as close as possible the solution gradient. The wall elements were designed in order to be compatible with the near-wall special shape function used by FIDAP 8.0 wall elements. The final aim of the mesh structure chosen was to obtain a numerical solution as independent as reasonably achievable from the mesh quality.

Two different openings were analyzed for each compensating connection in order to obtain a complete characterization of the three spools, covering the range of medium-large spool travel (0.3 and 0.5 mm).

The convergence criteria used to terminate the iterative process of solution was based on the control of both the solution and the residual vector. The convergence control was based on the evaluation of the relative error, and every solution was accepted when the tolerance became lower than $10^{-4}$ (in non-dimensional values).

The scale length chosen as reference for the non-dimensional problem statement was the metering section opening. The velocity scale of the problem was the estimated fluid velocity computed as the average speed in the section according to Eq. (6). In order to define the turbulent problem in closed form, the $k$-$\varepsilon$ model of turbulence, suitable for fully developed turbulent fields, was assumed.

All geometric configurations have been solved for just a single reference condition, defined by the imposition of a common reference Reynolds number ($Re_{REF}$=1149) to the flow and a non-dimensional, parabolic velocity profile at the inlet section. The two additional equations related to the $k$-$\varepsilon$ model were scaled as well, with constant boundary conditions on the $k$-$\varepsilon$ fields having typical values of the order of $10^{-5}$ and $10^{-9}$ respectively.

## 4 Flow Field Analysis and Characteristics Comparison

Figure 4 shows the velocity distribution in the six configurations investigated.

They condense (together with the pressure field and its differential $\Delta p$), all the information needed to get the four non-dimensional variables of Eq. (17), namely: flow rate $Q^*$, actual velocity module in the metering section $U_R^*$, jet flow angle $\theta_1$ and output main flow stream angle $\theta_2$.

Figure 4 shows the flow field in the three compensating profiles at 0.3 mm opening. Here it can be observed that the spool shape considerably affects the velocity distribution in a general sense, and close to the metering edge in particular.

The chamfer radius at the spool metering section actually imposes a jet flow angle of 50°-55°; conversely, if a 90° sharp edge is used, the Coanda effect induced by the wall, modifies the ideal flow behaviour, forcing the jet to stay closer than expected to the wall. The final jet flow angle can be estimated to be very close to 80°-85°. All the jet flow angles were obtained in the post processing phase as the averaged velocity vector angle in the turbulent core of the flow.

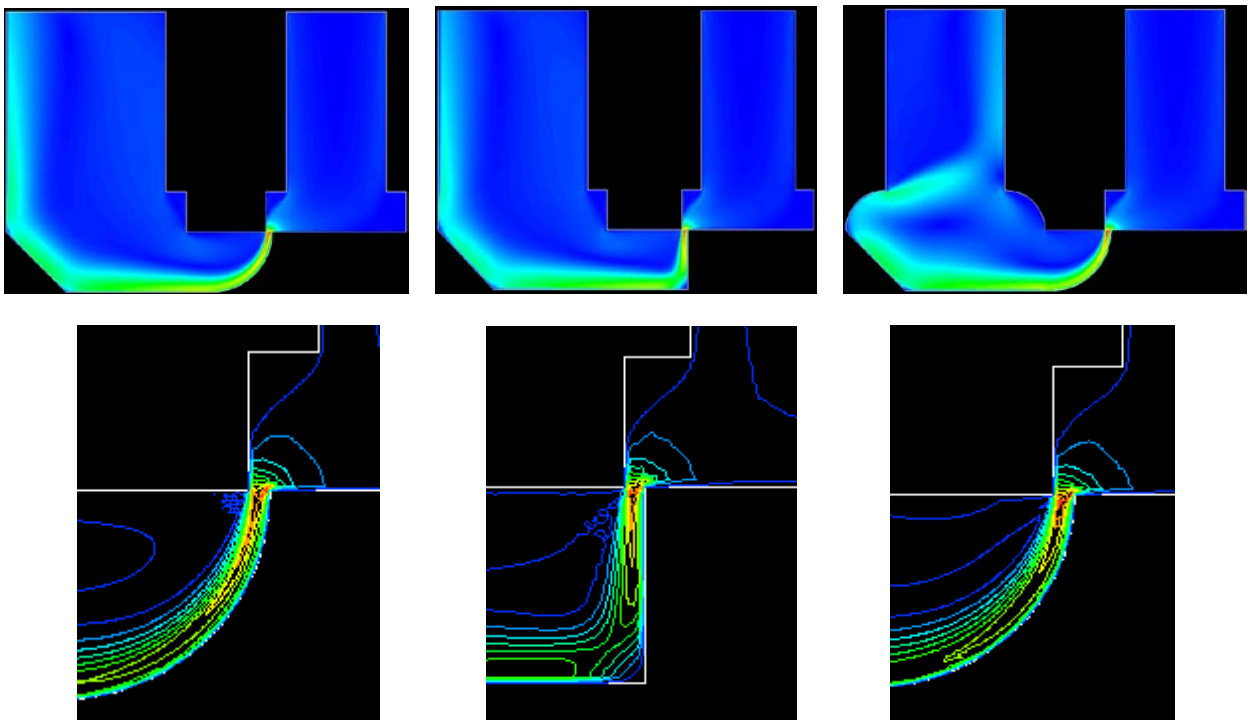

**Fig. 4:** *Non-dimensional absolute velocity distribution, 0.30 mm opening, and related zooms for metering edge. Cases A, B and C respectively from left to right*

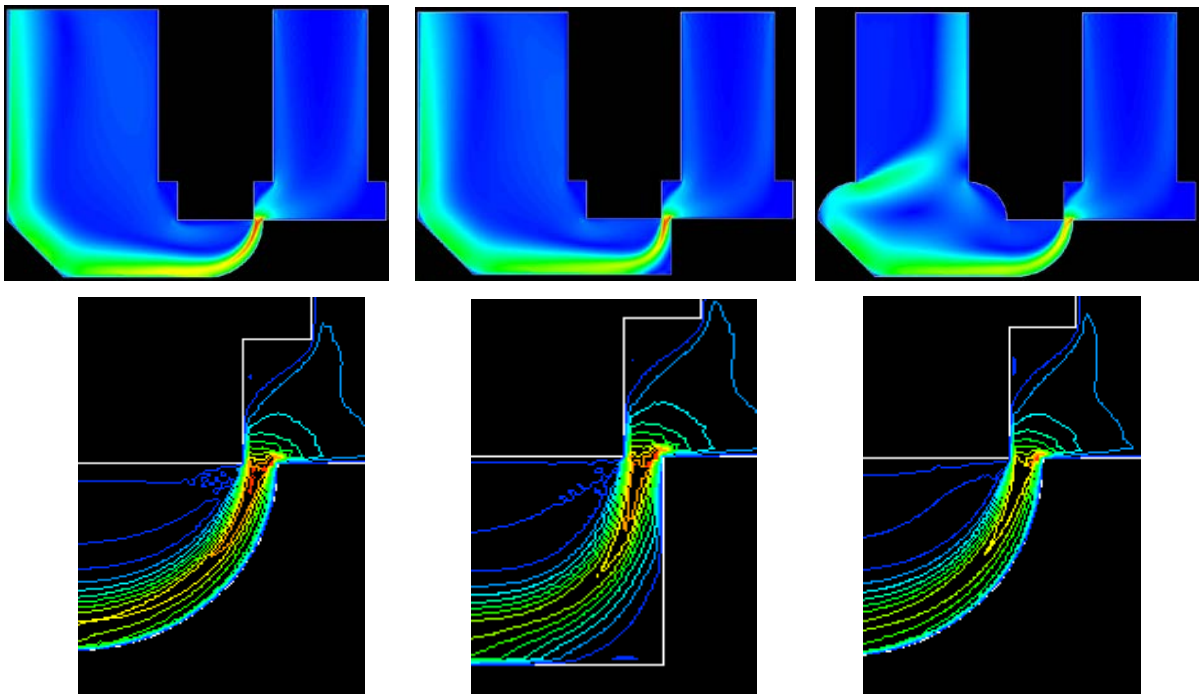

**Fig. 5:** *Non-dimensional absolute velocity distribution, 0.50 mm opening, and related zooms for metering edge. Cases A, B and C respectively from left to right.*

This fact confirms some conclusions presented by Lugowsky (1993), where the Coanda effect is indicated as the major cause of discrepancy between actual efflux and theoretical predictions. A further effect which can be of some interest, is the fact that the circulation induced in the valve land, has actually a limited effect on the valve outflow. The main jet flow, though deviated, directly enters the outlet section.

As far as the pressure distribution is concerned, in all the cases analyzed, the pressure drop is localized in a very small region across the metering edge. The only remarkable difference among the three cases is the obvious presence of the stagnation pressure recovery in the dead angle, at the bottom of the spool, in case B.

The effect of this last phenomenon is evidenced also by the shape of the velocity distribution curves in Fig. 4.

A further effect related to the pressure distribution is the pressure drop associated with a given flow rate. Although the three cases are conceptually identical, they show a different overall pressure drop. The maximum hydraulic resistance is offered by case B, and the minimum by case C.

The data related to the fluid flow are collected in Table 1, where the dimensionless values of flow rate, speed, pressure drop and angles are compared for the three geometries analyzed at 0.3 mm spool travel.

As already underlined, the maximum differences are shown in terms of jet angle at the metering section $\theta_1$, followed by the differences in velocity magnitude at the metering edge (5%) and in overall pressure drop (3%). The two values shown in the speed cells are referred to the averaged value in the main flow section (metering section minus the two boundary layers) and the peak value, respectively.

When the spool travel is changed from 0.3 to 0.5 mm, the flow field is modified as shown in Fig. 5.

Once more, the profile of the spool imposes angles of 50°-55° to cases A and C. In this latter case, the effect of the circulation becomes somehow more evident. The geometry of case B, as it might be easily expected, shows a completely different behavior from the previous case. The Coanda effect plays a different role, and the jet flow angle is limited to 60°-65°.

The pressure drop is once more concentrated at the metering section, confirming the validity of the assumption on which the procedure of Eq. (11) to (20) is based. It is worth noting, as it can be seen in Fig. 5, that the differences in efflux of case B enlarge considerably the extension of the zone with overall pressure increase due to stagnation.

The pressure drop evaluation confirms that the sharp edge geometry (case B) offers the maximum hydraulic resistance.

Comparing geometry A and C, the rating is reversed with respect to the 0.3 mm opening, and case C offers a higher hydraulic resistance compared to case A; this fact may be a consequence of the recirculating flow in the valve land.

The dimensionless values computed are summarized in Table 2, with the same structure of Table 1. The spread of values in angle $\theta_1$ is considerably reduced, but the difference in pressure drop is now 8%, substantially due to the better behavior of geometry A. The difference in speed value are about 10%, due to the high value shown by geometry C.

Summarizing the results, it is always possible to consider the discharge as a concentrated pressure drop, even in case of compensating geometry, and therefore the approximation implied by Eq. (4) can be used. As shown by Borghi, Cantore et al (1997),

**Table 1:** Non dimensional variables calculated for the three shapes analyzed, 0.30 mm opening.

| $L_{REF}$ = 0.30 mm, $Re_{REF}$ = 1149 | Non-Dimensional Values | | | Efflux Angles | |
|---|---|---|---|---|---|
| Mineral Oil | $Q^*$ | $U_R^*$ | $\Delta p^*$ | $\theta_1$ | $\theta_2$ |
| Rounded Edge Shape (Case A) | 6555.46 | 37.09/42.03 | 1388.9 | 50°/55° | 45° |
| Sharp Edge Shape (Case B) | 6555.46 | 38.18/43.27 | 1392.33 | 80°/85° | 45° |
| Rounded Edge/Body Chamber Shape (Case C) | 6555.46 | 36.45/41.31 | 1354.83 | 50°/55° | 45° |

**Table 2:** Non dimensional variables calculated for the three shapes analyzed, 0.50 mm opening.

| $L_{REF}$ = 0.50 mm, $Re_{REF}$ = 1149 | Non Dimensional Values | | | Efflux Angles | |
|---|---|---|---|---|---|
| Mineral Oil | $Q^*$ | $U_R^*$ | $\Delta p^*$ | $\theta_1$ | $\theta_2$ |
| Rounded Edge Shape (Case A) | 1410.07 | 13.32/15.10 | 192.05 | 50°/55° | 45° |
| Sharp Edge Shape (Case B) | 1410.07 | 13.53/15.33 | 207.69 | 65°/70° | 45° |
| Rounded Edge/Body Chamber Shape (Case C) | 1410.07 | 14.64/16.6 | 201.626 | 50°/55° | 45° |

**Table 3:** Discharge Coefficient and Flow Loss Resistance Variations with Compensating Connections Openings.

| | Rounded Edge Shape | | Sharp Edge Shape | | Rounded Edge & Circ. Chamber Shape | |
|---|---|---|---|---|---|---|
| Opening | $C_d$ | $K$ | $C_d$ | $K$ | $C_d$ | $K$ |
| 0.30 mm | 0.659 | 2.301 | 0.659 | 2.302 | 0.668 | 2.240 |
| 0.50 mm | 0.636 | 2.471 | 0.613 | 2.664 | 0.621 | 2.594 |

using this approximation it is easy to get reasonable estimates of resistance coefficient $K$ and efflux coefficient $C_d$. Using the non dimensional results of CFD runs the above mentioned quantities can be computed as:

$$K = 2 \cdot \Delta p^* \cdot \left( \frac{A_{TH}^*}{Q^*} \right)^2 \tag{21}$$

and:

$$C_d = \sqrt{\frac{1}{K}} \tag{22}$$

Table 3 collects the results obtained for the two spool positions presented here and the three geometric configurations. It is worth noting that the three cases have equivalent behaviour (only case C differs slightly) at the smaller opening, whilst the differences become bigger at 0.5 mm, where the values (generally lower) of $C_d$ range from 0.636 (case A) to 0.613 (case B).

Due to the duality of Eq. (21) and (22), the same considerations apply to resistance coefficient $K$.

## 5 Experimental Verification

One of the results of practical interest to the purpose of component design is the estimation of the flow force acting on the spool for a given position. This result can be derived from the non dimensional data presented in tables 1, 2 and 3.

Using Eq. (17), it is relatively easy to compute the non-dimensional axial component of the stationary flow force, and from that value to extend the estimate to the full range of operation of the valve by applying the re-scaling technique summarized in Eq. (18) to (20). The output of this process is a complete plot of $F$-$\Delta p$ curves at given spool position.

Figure 6 presents the curves computed for the three cases considered, compared with the experimental data obtained on a distributor with a geometry substantially similar to the one simplified in geometry A. The experimental activity was carried out by the authors using the set-up presented in Borghi et al (1997), recording stationary characteristics of the ports presented at fixed spool position and up to a hydraulic dissipation in the metering section of 60 kW.

It is worth noting that at 0.3 mm opening, the numerical prediction fits almost perfectly the experimental data for both geometry A and C. On the contrary, geometry B deviates considerably from the experimental evidence. This apparently surprising result can be easily understood looking at the structure of Eq. (17) and at the jet flow angle at 0.3 mm opening. In this position, geometry B evidences a jet flow angle very close to 90°, due to the Coanda effect; this causes the

contribution of $\cos\theta_1$ to become very small, and all the contribution to the term in brackets is due to the value of the out stream angle $\theta_2$. Since the geometry is considerably different from the one shown, the difference between the numerical and the experimental values are easily understood.

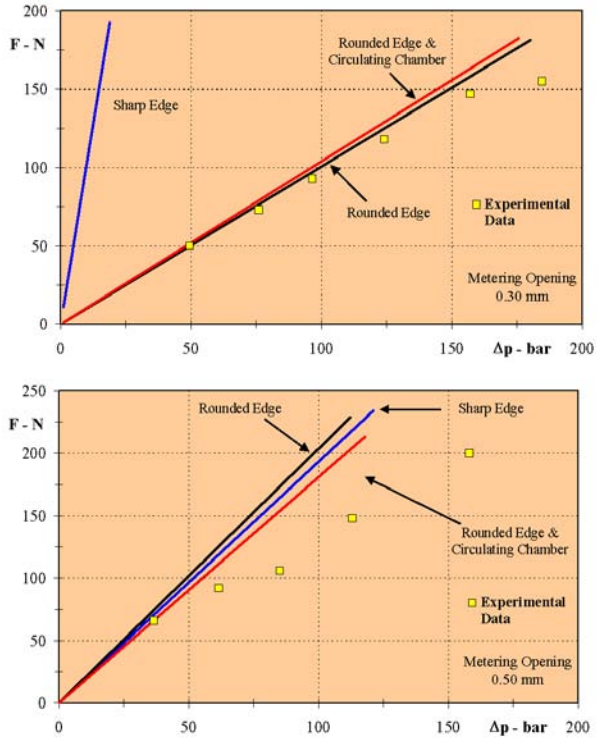


**Fig. 6:** *Axial Flow Force Prediction: Numerical Results versus Experimental Data Comparisons.*

This last comment could suggest that an output angle $\theta_2$ close to 90° could make the final axial flow force very small.

Unfortunately this is true only at very small openings, where the inlet jet angle is forced to be close to 90° as well. Since the compensation is made in order to have the valve compensated for the complete range of openings, this consideration is not applicable in general.

Looking at the results of geometry A and C, it is easy to notice that the presence of the circulating geometry of the land does not influence the final value of the axial flow force. This is due to the fact that the geometry actually constrains the values of the in- and out- jet flow angles, making any differences induced by the land geometry negligible.

Looking at the larger opening, the characteristic curves tend to get closer to each other, and geometry B shows a behaviour which is somehow intermediate. It is also worth noting that the effect of the circulation induced by the land, becomes more relevant in this case. The contribution of the circulating flow reduces the value of the net axial flow force, reversing the position of the curves with respect to the 0.3 mm opening.

However, it must also be noticed that the contrast between experimental data and numerical results in this case is definitely worse than in the previous one. The amount of this mismatch tends also to increase as the hydraulic power value increases. This effect was already noticed by the authors in Borghi, Cantore et al (1997), when the comparison was made for uncompensated connections and might be explained considering that.

Using and axis-symmetric approximation, the numerical run does not have the ability to catch any 3-D effect. This characteristic may have a negligible influence on small openings, where the value of the pressure upstream the metering edge tends to be uniform, but may not be negligible on larger openings;

As shown by the authors in Borghi, Milani et al (1998), the dynamic component of the flow forces, may account for 15 to 20% of the stationary force. If the contribution of the dynamic component is therefore opposing the stationary one, this may account for at least part of the difference between the experimental (total force) and the numerical (steady-state component) results.

The second point is a limitation of the test apparatus used, and induces a dynamic component in the steady-state analysis which was not removed and which is a potential source of errors.

## 6 Conclusions

The paper presented some results obtained applying numerical analysis based on Computational Fluid Dynamics (CFD) to three different valve port connection, commonly used to provide compensation to stationary axial flow forces. All the geometry were derived from port connections of an actual commercial distributor. The numerical activity was based on a simplified approach to geometry representation (axis-symmetric models) and on an analytical approach to non-dimensional problem statement.

The approach presented allowed a comprehensive characterization of the compensated port connections, from visualization of the fluid flow to determination of the non-dimensional variables needed to compute the value of the axial flow force on the spool.

Three main results may be considered a positive outcome of the procedure:

The three geometries show a general ability to compensate the axial flow force, and additional actions (chamber at the inlet section, circulating chamber in the land) have influence only in particular flow conditions;

The Coanda effect plays an important role at small openings and sharp-edged geometry, making actual flow considerably different from the theoretical one;

The design procedure has shown the ability to reproduce the experimental data to a reasonable good extent, in both compensated and uncompensated geometry.

Some aspects of the flow must be investigated in deeper detail. For instance the effect of the 3-D flow in actual geometry must be carefully checked, at medium and large openings in particular, in order to verify whether or not it can be claimed to be cause of some discrepancies in the numerical-experimental comparison. Nevertheless, the combined application of simpli-

fication in geometry and dimensional analysis showed to be a powerful and cost-effective procedure to the purpose of commercial valve design.

## Nomenclature

| | |
|---|---|
| $A$ | area |
| $C_A$ | area re-scale factor |
| $C_c$ | *vena contracta* coefficient |
| $C_d$ | discharge coefficient |
| $C_F$ | force scale factor |
| $C_v$ | velocity coefficient |
| $C_P$ | pressure scale factor |
| $C_Q$ | flow-rate scale factor |
| $C_U$ | velocity scale factor |
| $F$ | force |
| $k$ | turbulent kinetic energy |
| $K$ | concentrated loss factor |
| $L$ | length |
| $Q$ | flow-rate |
| $Re$ | Reynolds Number |
| $U$ | velocity |
| $\Delta p$ | pressure drop |
| $\beta(Re)$ | Reynolds Number ratio parameter |
| $\varepsilon$ | turbulent kinetic energy dissipation rate |
| $\nu$ | fluid cinematic viscosity |
| $\theta$ | efflux angle |
| $\rho$ | fluid density |

**Superscript**

| | |
|---|---|
| * | non-dimensional value |

**Subscript**

| | |
|---|---|
| TH | theoretical |
| R | actual |
| REF | reference |
| 1 | metering edge |
| 2 | compensation |

## References


**Blackburn, J. F., Reethof G., Shearer J. L.** 1960. *Fluid Power Control*. M.I.T. Technology Press & John Wiley & Sons.

**Merrit, H. E.** 1967. *Hydraulic Control Systems*. John Wiley & Sons.

**Patankar S. V.** 1980. *Numerical Heat Transfer and Fluid Flow*. Hemisphere Publishing Corporation.

**Idelchick** 1983. *Handbook of Hydraulic Resistance*. Springer-Verlag.

**Chapra, S. C., Canale, R. P.** 1989. *Numerical Methods for Engineers.* Second Edition, McGraw-Hill.

**Abbott M. B., Basco, D. R.** 1989. *Computational Fluid Dynamics: An introduction for engineers*. Longman Scientific & Technical. *FIDAP 8.0* 1998. *User's Manual*. Fluent Inc., Lebanon – NH, USA.

**Lugowsky, J.** 1993. Experimental Investigation on the Origin of Flow Forces in Hydraulic Piston Valves. *10th International Conference on Fluid Power*, BHR, Brugges, Belgium.

**Ferretti, G., Paoluzzi, R., Zarotti, G. L.** 1995. CFD Flow Analysis of Steady-State Flow Forces on Valves. *Proceedings of the 2nd ISFP*, Shanghai, China.

**Palumbo, A., Paoluzzi, R., Borghi, M., Milani, M.** 1996. Forces on a Hydraulic Valve Spool. *Proceedings of the Third JHPS International Symposium on Fluid Power* – pp. 543-548 - Yokohama, Japan.

**Borghi, M., Cantore, G., Milani, M., Paoluzzi, R.** 1997. Experimental and Numerical Analysis of Forces on a Hydraulic Distributor. *Proceedings of the Fifth Scandinavian International Conference on Fluid Power*, SICFP '97 – Vol. I – pp. 83-98 - Lingkoeping, Sweden.

**Borghi, M., Milani, M., Paoluzzi, R.** 1998. Transient Flow Forces Estimation on the Pilot Stage of a Hydraulic Valve. *Proceedings of the 1998 IMECE* - ASME *International Mechanical Engineering Congress and Exposition* - Fluid Power systems Technology Division – Anaheim, California, USA.

**Borghi, M., Cantore, G., Milani, M., Paoluzzi, R.** 1998. Analysis of Hydraulic Components Using Computational Fluid Dynamics Models - Paper C09297 - *Proceedings of the Institution of Mechanical Engineers* - Vol. 212 (7), Part C - *Journal of Mechanical Engineering Science* - pp. 619-629.

**Borghi, M., Milani, M., Paoluzzi, R.** 1999. Erosion Estimation in a Pressure Relief Valve by Means of Particle Tracking Analysis. *The Sixth Scandinavian International Conference on Fluid Power*, SICFP '99 – Tampere, Finland.

**Borghi, M., Milani, M., Paoluzzi, R.** 1999. Computational Fluid Dynamics in Solid Particle Estimation in Hydraulic Poppet Valves. *The 1999 SAE Off-Highway and Powerplant Congress & Exposition* - SAE PAPER 1999-01-2835 - Indianapolis, Indiana, USA.

**Borghi, M. , Milani, M., Paoluzzi, R.** 1999. Stationary and Dynamic Analysis of a Water Relief Valve. *The Fourth JHPS International Symposium on Fluid Power*, JHPS '99 – Ariake, Tokyo, Japan.

**MASSIMO BORGHI**
Born in Modena, 1956.
MSc in Mechanical Engineering at the University of Bologna in 1981. Researcher at the Faculty of Engineering of the University of Bologna in 1983 Associate Professor at the Faculty of Engineering of the University of Modena in 1998. Author and Co-Author of more than 40 paper dealing with Fluid Power machines and components, Energy Conversion Systems and Internal Combustion Engines.

**MASSIMO MILANI**
Born in Modena in 1968.
MSc in Materials Engineering at the University of Modena in 1994. PhD in Materials Engineering at the University of Modena in 1998. Researcher at the Faculty of Engineering of the University of Modena in 1999. Author of about 30 articles dealing with Fluid Power machines analysis and design, hydraulic components internal flow field analysis, CFD analysis of wall-particles interaction.

**ROBERTO PAOLUZZI**
Born in Ferrara in 1961.
MSc in Nuclear Engineering at the University of Bologna in 1986. Senior Researcher at Cemoter - C.N.R. Institute with interests in fluid power systems, control and simulation and in computational fluid mechanics. Italian National Secretary of ISTVS (International Society for Terrein-Vehicle Systems). Member of ASME and FPNI. Chairman of ISO/TC 127/SC 4 since 1991. Author of more than 120 papers and technical reports in fluid power systems technology and Earth Moving Machinery parts and components design.